DOI: 10.1002/ ((adhm.201800983))
Article type: Full Paper

Replacement of Rat Tracheas by Layered, Trachea-like, Scaffold-free Structures of Human Cells Using Bio-3D Printing System

*Ryusuke Machino, Keitaro Matsumoto, Daisuke Taniguchi, Tomoshi Tsuchiya, Yosuke Takeoka, Yasuaki Taura, Masaaki Moriyama, Tomoyuki Tetsuo, Shosaburo Oyama, Katsunori Takagi, Takuro Miyazaki, Go Hatachi, Ryoichiro Doi, Koichiro Shimoyama, Naoto Matsuo, Naoya Yamasaki, Koichi Nakayama, Takeshi Nagayasu**

Dr. R. Machino, Dr. K. Matsumoto, Dr. D. Taniguchi, Dr. T. Tsuchiya, Dr. Y. Takeoka, Dr. Y. Taura, Dr. M. Moriyama, Dr. T. Tetsuo, Dr. S. Oyama, Dr. K. Takagi, Dr. T. Miyazaki, Dr. G. Hatachi, Dr. R. Doi, Dr. K. Shimoyama, Mt. N. Matsuo, Dr. N. Yamasaki, Prof. T. Nagayasu
Department of Surgical Oncology, Nagasaki University Graduate School of Biomedical Sciences, Nagasaki, 852-8501, Japan
Medical-engineering hybrid professional development center, Nagasaki University Graduate School of Biomedical Sciences, Nagasaki, 852-8501, Japan
E-mail: nagayasu@nagasaki-u.ac.jp
Prof. K. Nakayama
Department of Regenerative Medicine and Biomedical Engineering Faculty of Medicine, Saga University, Saga, 840-8502, Japan

Keywords: tracheal regeneration, bio-3D printer, tissue engineering, scaffold-free, bioengineered organ

Current scaffold-based tissue engineering approaches are subject to several limitations, such as design inflexibility, poor cytocompatibility, toxicity, and post-transplant degradation. Thus, scaffold-free tissue-engineered structures could be a promising solution to overcome the issues associated with classical scaffold-based materials in clinical transplantation. The present study seeks to optimize the culture conditions and cell combinations used to generate scaffold-free structures using a bio-3D printing system. Human cartilage cells, human fibroblasts, human umbilical vein endothelial cells, and human mesenchymal stem cells from bone marrow were aggregated into spheroids and placed into a bio-3D printing system with dedicated needles positioned according to 3D configuration data to develop scaffold-free trachea-like tubes. Culturing the bio-3D-printed structures with proper flow of specific medium in a bioreactor facilitated the rearrangement and self-organization of cells improving

physical strength and tissue function. The bio-3D-printed tissue formed small-diameter trachea-like tubes that are implanted into rats with the support of catheters. It is confirmed that the tubes are viable *in vivo* and that the tracheal epithelium and capillaries proliferated. This tissue-engineered, scaffold-free, tubular structure can represent a significant step towards clinical application of bioengineered organs.

1. Introduction

The trachea is essential for respiration, phonation, and airway protection. Thus, if it narrows or collapses, it is life-threatening.[1–3] Safe, resectable tracheal ranges are approximately half the length in adults and one third the length in children.[4,5] A variety of tracheal replacement strategies have been reported, including artificial prostheses,[6,7] autografts,[8] native or decellularized allografts,[9] and autologous grafts of tissue-engineered constructs.[10–12] However, all these methods have shortcomings. Acellular tracheal prostheses often cause tissue granulation, implant migration, progressive scar formation, and restenosis.[13] Autografts and allografts undergo remodeling upon implantation, due to their limited availability and poor mechanical properties, this leads to collapse, scarring, and airway occlusion. [4] The use of allogeneic donor tissues can cause disease transmission and immunogenicity. Immune response issues can be avoided using tissue-engineered constructs comprising autologous cells in scaffolds, but the scaffolds lack design flexibility and the cytocompatibility of natural materials and may trigger a host response to toxic byproducts released during their degradation.[14] Thus, new techniques for producing scaffold-free tissue-engineered constructs are required.

One of our coauthors (K. Nakayama) developed a novel, robotic bio-3D printing system, “Regenova,” which allows to produce 3D cellular structures using multicellular spheroids in needle arrays placed according to pre-designed data.[15] This system succeeded in producing

vessel-like structures, but they are physiologically distinct from other organs.[16] The vessels obtained oxygen and nutrients via blood flow through the structure interior, while other tubular organs generate their own blood vessels after *in vivo* implantation. Different approaches are necessary to create viable tubular organs. Therefore, we focused on the fact that support cells, such as fibroblasts[17] or mesenchymal stem cells[18,19], induce endothelial cells to form capillary-like structures in 3D co-cultures. Using a similar method, our coauthors successfully performed the autologous transplant of neo-cartilage structures made of primary cultured cells to rat cervical tracheas.[20]

In this study, we attempted to generate neo-cartilaginous tubes and neo-fibrous tubes by co-culture of human chondrocytes, human mesenchymal stem cells (MSCs), human fibroblasts, and human umbilical vein endothelial cells (HUVECs) using previously reported methods.[20] Additionally, we attempted to build a structure more similar to that of the native trachea with strength suitable for rat transplant.

2. Results

2.1 Cartilaginous tubes

2.1.1 Gross morphological assessment and biomechanical analysis of cartilaginous tubes

Cartilaginous tubes were formed by 7 groups of spheroids. Group C-I consisted exclusively of normal human articular chondrocytes (NHACs). Group C-II consisted of NHACs and HUVECs. Group C-III consisted of NHACs, HUVECs, and MSCs; this group was further divided into groups C-IIIa, C-IIIb, and C-IIIc each containing a different ratio of NHACs and MSCs. Group C-IV consisted of HUVECs and MSCs. Group C-V consisted exclusively of MSCs (see **Table S1** for details). The structures in groups C-I and C-V were weaker and more difficult to handle than those of other groups, owing to their thinness (**Figure 1a–g**). The thickness and length of the structures at the time of bio-3D printing were approximately 550 μm and 5 mm, respectively for all groups. After 35 days of culture, the thickness of the

different groups were: C-I, 0.56 ± 0.09 mm; C-II, 0.75 ± 0.06 mm; C-IIIa, 0.60 ± 0.16 mm; C-IIIb, 0.86 ± 0.03 mm; C-IIIc, 0.76 ± 0.25 mm; C-IV, 0.81 ± 0.07 mm; C-V, 0.69 ± 0.16 mm. There were no significant differences between the thicknesses values among the groups (**Figure 1h**).

The lengths of the different groups were: C-I, 4.37 ± 1.19 mm; C-II, 3.15 ± 1.65 mm; C-IIIa, 2.96 ± 0.30 mm; C-IIIb, 1.95 ± 0.41 mm; C-IIIc, 2.17 ± 0.17 mm; C-IV, 1.54 ± 0.27 mm; C-V, 1.81 ± 0.70 mm. The thickness and length of group C-I remained unchanged after 35 days of culture. However, as the proportion of MSCs in the structures exceeded 40%, the lengths tended to shorten significantly (**Figure 1i**).

The force at failure and ultimate tensile strength (UTS) of the different groups were: C-I, 92.25 ± 77.22 mN and 38.78 ± 29.69 kPa; C-II, 420.66 ± 151.45 mN and 190.96 ± 67.35 kPa; C-IIIa, 460.50 ± 294.05 mN and 290.63 ± 164.62 kPa; C-IIIb, 283.20 ± 95.27 mN and 188.58 ± 74.20 kPa; C-IIIc, 294.67 ± 159.72 mN and 207.64 ± 107.11 kPa; C-IV, 158.00 ± 134.95 mN and 107.75 ± 87.56 kPa; C-V, 27.33 ± 22.01 mN and 21.86 ± 15.28 kPa. Group C-IIIa exhibited a significantly higher force at failure and UTS compared to other groups (**Figure 1j, k**). The structures printed from spheroids of NHACs and MSCs collapsed during culture and were not evaluated (data not shown).

2.1.2 Biochemical analysis of cartilaginous tubes

Glycosaminoglycan (GAG) content and GAG content normalized to DNA content of the different groups were: C-I, 37.05 ± 7.30 μg/ml and 49.72 ± 13.88 μg/μg; C-II, 30.45 ± 1.80 μg/ml and 74.05 ± 18.99 μg/μg; C-IIIa, 29.45 ± 5.00 μg/ml and 86.04 ± 17.67 μg/μg; C-IIIb, 35.06 ± 5.89 μg/ml and 70.04 ± 20.51 μg/μg; C-IIIc, 30.05 ± 3.08 μg/ml and 78.88 ± 32.93 μg/μg; C-IV, 15.18 ± 10.02 μg/ml and 67.36 ± 18.83 μg/μg; C-V, 3.89 ± 2.31

μg/ml and 62.29 ±24.31 μg/μg. Groups C-IV and C-V that did not include NHACs had lower GAG and DNA content (an indirect measure of cell number) than the other groups (**Figure 1l, m**). The groups that included NHACs showed no significant difference in GAG content or GAG/DNA among them (**Figure 1l, n**).

2.1.3 Histology and immunohistochemistry of cartilaginous tubes

Although NHACs were not included in groups C-IV and C-V, deposition of GAG was detected in all groups by Alcian blue staining (**Figure 2a, e, I, m, q, u, y**). Similarly, collagen II was detected in all groups (**Figure 2b, f, j, n, r, v, z**). However, the area of collagen II detection was narrower in group C-V than in the other groups (**Figure 2b, f, j, n, r, v, z**). Collagen IV was not detected in group C-V (**Figure 2aa**), while the groups that included HUVECs had the same amount at the time of bio-3D printing, positive cells for the endothelial marker cluster of differentiation (CD) 31 ($CD31^+$ cells) were broadly detected in groups C-IIIa, C-IIIb, and C-IIIc; and only slightly detected in groups C-II and C-IV(**Figure 2d, h, l, p, t, x, bb**).

2.2 Fibrous tubes

2.2.1 Gross morphological assessment and biomechanical analysis of fibrous tubes

Fibrous tubes were formed by 4 spheroid groups. Group F-I consisted exclusively of normal human dermal fibroblasts (NHDFs). Group F-II consisted of NHDFs and HUVECs. Group F-III consisted of NHDFs and MSCs. Group F-IV consisted of NHDFs, HUVECs, and MSCs (see **Table S1** for details). The thickness and length of the structures at the time of bio-3D printing were approximately 550 μm and 5 mm, respectively, in all groups. After 35 days of culture, the thickness and length of the different groups were: F-I, 0.81 ± 0.04 mm and 3.27 ± 0.46 mm; F-II, 0.84 ± 0.13 mm and 2.53 ± 0.30 mm; F-III, 0.91 ± 0.09 mm and 2.88 ±

0.25 mm; F-IV, 0.85 ± 0.16 mm and 3.51 ± 0.57 mm. The values were similar across the 4 groups **(Figure 3e, f)**. The force at failure and UTS of the different groups were: F-I, 209.33 ± 45.65 mN and 77.67 ± 3.30 kPa; F-II, 201.50 ± 103.32 mN and 101.35 ± 60.76 kPa; F-III, 218.80 ± 65.67 mN and 79.32 ± 24.22 kPa; F-IV, 448 ± 32.04 mN and 155.99 ±33.06 kPa. Mechanical analysis of the uniaxial tension revealed that the force at failure depended on the cell combination used to generate the spheroids. For instance, group F-IV exhibited a tensile strength significantly higher than that of other groups (**Figure 3g**). A similar phenomenon was observed for the UTS (**Figure 3h**).

2.2.2 Histology and immunohistochemistry of fibrous tubes

Masson's trichrome staining showed abundant and thick collagenous fiber bundles in the outer layers of the structures (**Figure 4a, f, k, p**) and a pronounced collagen deposition was observed in the outer layers of all groups upon Fast Green/Picrosirius Red staining (**Figure 4b, g, l, q**). Polarized light microscopy showed that the collagenous fiber bundles mostly consisted of large collagen fibers and that the fiber bundles in group F-IV were broader and longer than those of other groups (**Figure 4c, h, m, r**). Collagen IV was detected in the central areas of all structures (**Figure 4d, I, n, s**). CD31 was detected in the central regions of group F-II structures and throughout F-IV structures (**Figure 4e, j, o, t**). Furthermore, small luminal $CD31^+$ cell aggregates were observed in group F-IV but not in group F-III structures (**Figure 4j, t**).

2.3 Trachea-like tubes

2.3.1 Gross morphological assessment and biomechanical analysis of trachea-like tubes

Immediately after bio-3D printing, the spheroids of group F-IV were indistinguishable from those of group C-IIIa. After 7 days of culture, trachea-like tubes were distinguishable,

forming laminar structures of F-IV and C-IIIa rings (**Figure 5b;** with Kenzan, **Figure 5c;** without Kenzan, F-IV ring, orange; C-IIIa ring, yellowish-white). However, after 35 days of culture, the trachea-like tubes lost its laminar appearance and acquired an orange coloration (**Figure 5d**).

The thickness and length of the trachea-like tubes harvested after 35 days of culture were 0.81 ± 0.23 mm and 3.79 ± 1.11 mm, similar to those of the fibrous tubes (group F-IV) and higher than those of cartilaginous tubes (group C-IIIa) and native rat tracheas (0.40 ± 0.08 mm thick and 2.35 ± 0.25 mm long)(**Figure 5e, f**). The UTS of the trachea-like tubes was 258.23 ± 173.60 kPa, significantly less than that of native rat tracheas (878.44 ± 137.15 kPa)(**Figure 5h**). However, their force at failure was 683.0 ± 259.32 mN, showing no significant difference to that of native rat tracheas, but significantly higher than that of the cartilaginous and fibrous tubes (**Figure 5g**).

2.3.2 Biochemical analysis of trachea-like tubes

GAG content in the trachea-like tubes was 50.93 ± 9.12 μg/ml, significantly higher than that in the fibrous and cartilaginous tubes; however, the GAG content of native rat tracheas was 101.39 ± 8.37 μg/ml, much higher than that of the trachea-like tubes (**Figure 5i**). In contrast, DNA, an indirect measure of cell number, was significantly more abundant in the trachea-like tubes than in the cartilaginous tubes and the native rat tracheas (**Figure 5j**). GAG content normalized to DNA content in the trachea-like tubes was 43.1 ± 11.07 μg/μg, significantly lower than in cartilaginous tubes and native rat tracheas (**Figure 5k**).

2.3.3 Histology and immunohistochemistry of trachea-like tubes

Trachea-like tubes harvested after 35 days of culture were subjected to various stains. Hematoxylin-eosin staining, used to visualize cellular organization, showed that the cells were

aligned with the outer structure layer, but apparently did not align with the inner layer, where cell density was lower (**Figure 6a**). The laminar appearance of the trachea-like tubes might become incomprehensible because of this phenomenon. Extensive extracellular matrix (ECM) production was observed throughout the structures by Masson's trichrome staining (**Figure 6b**). Although the trachea-like tubes consisted of alternating F-IV and C-IIIa rings, Alcian blue staining was detected evenly inside the structures, and the differences between F-IV and C-IIIa rings were undetectable (**Figure 6c**). Similarly, collagen II and IV were equally identified inside the structure (**Figure 6d, e**). In contrast, small luminal $CD31^+$ cell aggregates were observed only in F-IV ring areas, although C-IIIa rings also contained HUVECs (**Figure 6f, g**).

2.3.4 Remodeling of the trachea-like tubes after transplantation

Seven days after transplantation the surfaces of the trachea-like tubes were covered in granulation tissue with small blood vessels, and their borders with the native rat tracheas were indistinguishable (**Figure 7c**). In contrast, 35 days after transplantation, the structures had shrunk, and the granulation tissue was less apparent (**Figure 7d**).

Seven days after transplantation, the trachea-like tubes had small luminal $CD31^+$ cell aggregates (**Figure 7f**) and 35 days after transplantation, the $CD31^+$ cells surrounded a larger lumen (**Figure 7k**). The presence of pan-cytokeratin positive epithelial cells on the luminal side of the trachea-like tubes was confirmed 35 (**Figure 7l**) but not 7 days after transplantation (**Figure 7g**). Epithelial cells were not included in the spheroids, so these cells probably migrated from the native rat tracheas. Alcian blue (**Figure 7h, m**) and collagen II (**Figure 7i, n**) staining became more evident in the trachea-like tubes over time.

3. Discussion

The trachea is formed by various cells types and tissues that provide its specific functions.[21] Many trachea regeneration trials have been reported; however, most required scaffolds. The use of scaffolds in the airway produces negative effects after *in vivo* transplantation.[22,23] Therefore, artificial tracheas without scaffolds are preferred. Several methods have been previously reported to generate tubular structures from cells. For instance, scaffold-free tissue-engineered blood vessels have been generated by cell sheet engineering. However, these approaches require repeated attempts and culture times of nearly 6 months before transplantation.[24] Similarly, other studies have attempted to use multicellular spheroids to generate scaffold-free tubular structures; however, these studies used molds to fuse spheroids and were thus limited to structures with specific shapes.[23,25,26]

We previously reported the convenience of scaffold-free isogenic artificial tracheas produced by the bio-3D printing system in rats.[20] This previous report showed the potential of scaffold-free organs for clinical applications. However, the quality, strength, and maturation of bio-3D-printed scaffold-free structures vary according to cell source, species, and animal age.[16,20,27] Thus, it is necessary to investigate the quality and combination of the cells as well as the human cell and tissue culture conditions for clinical applications.

In this study, we investigated the function of artificial tracheas made with human cells. We found that spheroids consisting of fibroblasts, HUVECs, and MSCs contributed to the flexibility and bloodstream of the structures, while spheroids composed of chondrocytes, HUVECs, and MSCs added to their rigidity. Combinations of the two spheroid types produced artificial tracheas with properties more similar to the native ones. Furthermore, the artificial tracheas functioned under immunosuppressive treatment for an extended period after transplantation procedures to replace sections of native tracheas in rats. Epithelium extension from the native tracheas and blood vessel connections between microvessels of neighbor tissues were confirmed.

During transplantation, the structure was strong enough to be sutured, but failed to maintain its shape after enduring continuous breathing for extended time periods, increasing mortality risk. Silicone stents were used to prevent collapse after transplantation, as described previously.[20] It took sufficient time for the surrounding tissues to connect to the transplanted artificial tracheas by appropriate vasculogenesis. In this study, we did not remove the stents after maturation of the artificial tracheas to avoid mortality risk in the rats, and we intend to focus on this issue in future works. Granulation, an adverse effect of stent use, was observed only slightly in this study, even though epithelial cells did not completely cover the inner surface of the lumen. This may be owing to the fact that our procedure was different from that of autologous transplantation, the fact that artificial and native tracheas were from different species, or immunosuppressant effects.[28]

In the present study, three structures were evaluated according to mechanical strength and histological findings *in vitro* to choose the most appropriate for transplantation in rats. A cartilaginous tube, a fibrous tube, and a trachea-like tube that imitated 4 rings of the cartilaginous and fibroblast cell-based structures. The trachea-like tubes had the highest tensile strength, though the difference was not significant. Furthermore, although the GAG /DNA production of the trachea-like tubes was less than that of the cartilaginous tubes, the GAG production by the whole trachea-like tubes was greater. Because the strength of the entire structure was the most important aspect, the trachea-like tubes were chosen for transplantation.

The trachea-like tubes were weaker than native tracheas of 9-week-old rats; however, we expected that the structures would gain strength after *in vivo* maturation supported by a stent.[20] The trachea-like tubes were probably stronger than the cartilaginous and fibrous tubes because of growth factor production by fibroblasts, ECM production by cartilaginous cells, or differentiation of MSCs into cartilaginous cells.[29] Thus, spheroids consisting of four

cell types should be stronger. however, such complex structures were not examined in the present study; we will investigate them in the future.

In vivo maturation of the structures requires neovascularization, connecting microvessels in the structures, and native vasculature after transplantation.[20] In the present study, some lumens contained $CD31^+$ cells 7 days after transplantation, and the cells surrounded a larger lumen after 35 days. To aid vascularization in *vivo*, HUVECs were included in both structures, these cells formed microvascular networks containing $CD31^+$ cells *in vitro* and displayed many small vessel-like luminal structures. This inclusion may have positively affected the tensile strength of the structures because of ECM production. Blood vessel connections between microvessels in the structures and native vessels in the neighboring tissue were confirmed. The structures consisting human cells formed connections between their own vascular networks and those of the rat tissues around the tracheas, as observed in autografts.[20] Thus, the connection of the vasculature can occur even in tissues of different species, and HUVECs could become a cell source for vascularization of these 3D structures. Cartilaginification of the structures after transplantation did not occur in the present study as it did in previous reports[20] where cartilage was observed in the structures 23 days after transplantation. This may have been because the human chondrocytes used in this study were not primary cultured chondrocytes but had a partial fibroblast character because of rapid dedifferentiation during monolayer culture, resulting in a fibroblast-like phenotype that produced less cartilage than primary cells.[30] A previous study reported that aortic allografts with MSCs were transplanted to rabbit cervical tracheas supported with silicone stents. Fifteen months after transplantation, cartilaginous rings were confirmed around the grafts.[31] Thus, longer-term culture in the *in vivo* environment may be required for cartilage maturation. Nevertheless, our Bio-3D printing system produced trachea-like tubes without differentiation instructions and with epithelium reproduction 35 days after transplantation.

Our data show that the cartilaginous tube consisting of only chondrocytes (group C-I tubes) was too weak for transplantation. Therefore, other cell types were needed to strengthen the structures. One promising cell source was MSCs. However, a significant drawback is that these cells produce cartilage after chondrogenic induction which can lead to further hypertrophy and calcification. Additionally, they are expensive.[32] Recent studies have demonstrated that co-culture of articular chondrocytes (ACs) and MSCs mitigates these problems, as interactions between them maintain their chondrogenic phenotypes, resulting in robust chondrogenesis and minimized need for mature chondrocytes.[33–35] Additionally, although induction medium commonly supplemented with known chondrogenic factors, such as Transforming Growth Factor (TGF)- β, is usually needed for MSC differentiation to chondrocytes, co-culture with ACs in 3D conditions did not require these factors.[36, 37] In the 3D conditions of our study, collagen II and GAG production were confirmed in the group C-V tubes, suggesting chondrocytic differentiation of MSCs without supplements. However, the structures in this group were small, and their tensile strength was low. Only groups C-IV and C-V showed significant differences in GAG content among the chondrocyte groups, although the content ratio of chondrocyte cells was inverted. The spheroids consisting of only NHACs and MSCs were unable to maintain tubular structures for a long time after 3D printing. Therefore, it was suggested that MSCs should be used instead of NHACs and that HUVECs could promote effective chondrocytic differentiation of MSCs. We used a cell source ratio of 7:2:1 of chondrocytes:HUVECs:MSCs for the cartilage rings in the trachea-like tubes because the tensile strength of group C-IIIa tubes was higher than that of the other groups, and its GAG content and GAG/DNA content were similar to that of any group besides C-IV and C-V. The cell source ratio of the fibrous membrane matched that of the cartilage rings.

Regarding the distribution of ECM in the cartilaginous tube, collagen IV accumulated in the central area in all groups except group C-V, suggesting that adhesion between the ECM and adjacent cells is bolstered by long-term culture. This may increase the stability and tensile

strength of the structures because collagen IV increases structural integrity, stability, and function.[38] Furthermore, collagen IV, present in the central area, forms an insoluble network that plays a structural role in the basement membrane [39] that may be necessary for epithelialization of the cylindrical structures after implantation.

A similar analysis was carried out to determine the cell combination for the fibrous tubes whose tensile strength depended on the cell types and ratios in the spheroids. Several reports indicated that the proliferation and differentiation of cell-derived tissue in 3D culture vary based on cell content. In fibroblast/HUVEC co-cultures, fibroblasts presence decreased the apoptosis level of endothelial cells[40] and generated an ECM, essential for luminal differentiation,[17] whereas HUVECs formed multi-cell microvessels in spheroids.[41] In MSC/fibroblast co-cultures, MSCs promoted fibroblast proliferation and pro-collagen production,[42] whereas endothelial cells regulated the MSC activity,[43] migration,[44] and differentiation,[18] required to stabilize newly formed vasculature. Group F-IV tubes had broader and longer fiber bundles than the other groups. As a result, the structure consisting of fibroblasts, HUVECs, and MSCs had the highest mechanical strength and was chosen for the fibrous ring.

The Bio-3D printing system used in the present study provides several benefits, including compatibility with multiple spheroid types, ability to generate various 3D forms, and enough medium circulation around the assembled spheroids to support the cells until tissue maturation. Compared to the conventional forms of 3D printing, our method has two particular advantages. First, the Bio-3D printer can be used to make structures without folds, and, second, the structures generated by this technique develop sufficient strength within a month. Despite these advantages, the molecular mechanisms underlying the pattern and distribution of ECM proteins require further investigation.

The present study has some limitations. First, although the fabricated tubes were small (4 mm long and 1.7 mm inner diameter), many cells and long culture times were needed. A larger

model, like human tracheas, would require significantly more cells and a longer culture period. Further studies must be conducted using mass culture and larger spheroids to decrease the printing time. Second, the structures were observed for only one month *in vitro* and *in vivo*. Third, several other primary cell types, including smooth muscle cells, and their combination in different ratios, may have improved the structures but were not investigated. Finally, the strength of the trachea-like tubes was lower than that of the native trachea. To overcome this, the use of differentiation-inducing factors causing MSCs to form neo-cartilage cells might be needed- However, these factors require extensive culture times. In future studies, we will try to develop artificial tracheas that are stronger than the native ones without using differentiation-inducing factors.

Nevertheless, our study provides basic information on the formation of structures by human cell spheroids using a bio-3D printing system. This approach may lead to the production of complete human cell grafts for implantation of various tubular tissues without using foreign materials.

4. Conclusion

This study optimized the culture conditions and cell combinations used to produce scaffold-free structures with a bio-3D printing system and generated scaffold-free trachea-like tubes to replace the epithelium and capillaries lost because of surgical resection of rat tracheas. These engineered structures could represent a significant step towards the clinical application of bioengineered organs.

5. Experimental Section

5.1. Experimental design

This study describes the formation of artificial tracheas. To make such tracheas with a ladder structure, two types of bio-3D-printed tubes were constructed (cartilaginous and fibrous) to

form a ladder structure. The cartilaginous tubes consisted of chondrocytes with or without MSCs and HUVECs. The fibrous tubes consisted of fibroblasts with or without MSCs and HUVECs. Combinations of different cells types were seeded into micro-wells to form the spheroids used to construct the multicellular tubes. Trachea-like tubes with ladder structures were made by stacking alternating tube types using a bio-3D printing system (Regenova; Cyfuse, Tokyo, Japan). Cartilaginous tubes, fibrous tubes and trachea-like tubes were cultured for 35 days *in vitro* and then analyzed to select the one with the most favorable values of stiffness and elasticity. The chosen type was transplanted into rats, replacing a section of the native trachea (**Figure 8**).

5.2. Cell culture

NHDFs (CC-2509; Lonza, Inc., Walkersville, MD, USA) were grown in fibroblast cell growth medium supplemented with human fibroblast growth factor-beta (hFGF-β), insulin, fetal bovine serum (FBS), and gentamicin/amphotericin-B (FGM2 Bullet Kit; Lonza, Inc., Walkersville, MD, USA). NHACs (CC-2550; Lonza, Inc., Walkersville, MD, USA) were grown in chondrocyte growth medium containing R3-insulin-like growth factor-1 (R3-IGF-1), human recombinant fibroblast growth factor-beta (hrFGF-β), transferrin, insulin, FBS, and gentamicin/amphotericin-B (CGM Bullet Kit; Lonza, Inc.). HUVECs (C2517A; Lonza, Inc., Walkersville, MD, USA) were grown in endothelial cell growth medium containing human epidermal growth factor (hEGF), vascular endothelial growth factor (VEGF), R3-insulin-like growth factor-1, ascorbic acid, hydrocortisone, hFGF-β, heparin, FBS, and gentamicin/amphotericin-B (EGM-2 Bullet Kit; Lonza, Inc.). Human bone marrow-derived MSCs (PT-2501; Lonza, Inc., Walkersville, MD, USA) were grown in mesenchymal stem cell growth medium (PromoCell GmbH, Heidelberg, Germany). All media were supplemented with 100 U/mL penicillin-streptomycin (Thermo Fisher Scientific, Waltham, MA, USA).

All cell lines were cultured on 150 mm tissue culture dishes (TPP, Trasadingen, Switzerland), and maintained in a humidified cell culture incubator at 37 °C under a 5% CO_2 atmosphere.

5.3. Preparation of multicellular spheroids

Cell cultures were washed with phosphate buffered saline solution (PBS; Wako, Osaka, Japan), treated for 3 min with 0.25% trypsin (Nacalai Tesque, Kyoto, Japan), and centrifuged at 166 x *g* for 5 min. The resulting pellets were resuspended in each cell-type-specific medium. Afterward, we classified the chondrocyte- and fibroblast-based spheroids into seven and four groups, respectively, depending on the cell ratio (groups C-I – C-V; and groups F-I – F-IV; see Table S1 details). The mix rate of fibroblast cellular suspensions was matched with that of the cartilaginous tubes. Cell mixtures were plated at 2×10^4 cells/100 μL in a well of ultra-low adhesion, round-bottom, 96-well plates (Sumitomo Bakelite, Tokyo, Japan) and cultured for 48 h to generate cell spheroids.

5.4. Bio-3D printing

Three-dimensional printing data were prepared using the Cyfuse's software for 16-level tubular models of cartilaginous, fibrous, and trachea-like tubes, requiring 388 spheroids each. The model of the trachea-like tubes consisted of two spheroid kinds; the first 2-level ring model consisted of group F-IV spheroids (F-IV ring) and the second 2-level ring model consisted of group C-IIIa spheroids (C-IIIa ring), this ring combination was repeated four times. Nine-by-nine needles (Kenzan; Cyfuse) were positioned to act as a temporary scaffold during spheroid agglutination. The needles were made of stainless steel with diameters of 170 μm and pitches of 400 μm; a hole was left at the center of the scaffold. As described previously, the bio-3D printer (Cyfuse) made the tubular structures automatically, using the spheroids in the plates. Briefly, it picked up spheroids by vacuum through a suction nozzle (outer diameter 0.45 mm and inner diameter 0.23 mm) from each well and skewered them to

the designed depths of the needles. In the present study, smaller spheroids were difficult to handle with the robotic nozzle, so the spheroid size was set accordingly. A total of 388 spheroids were used to create the 3D tubular shape according to pre-designed 3D data (**Figure 8**). The time required for the placement of the 16-level structures was approximately 1.5 h.

5.5. Maturation of tubular structures

The 3D-printed, tubular structures in the needle arrays were cultured with proper medium flow (200 mL/h) in a bioreactor (Figure 8) inside a humidified cell culture incubator at 37 °C under 5% CO_2 for 7 days, at this time, the 3D shapes were self-sustaining, and the needle arrays were removed. The structures were transferred to 1.7 mm outer diameter plastic catheters (TERUMO, Tokyo, Japan). Further culturing was enforced with the proper medium flow (200 mL/h) in a bioreactor for 28 days with media changes every 3–4 days (**Figure 8**). The flow speed was chosen to avoid structural damage due to shear stress. The media ratio for cartilaginous tubes was set at 1:1 CGM:EGM2, for fibrous tubes at 1:1 FGM2:EGM2, and for trachea-like tubes at 1:1:1 CGM:FGM2:EGM2.

5.6. Morphological and biomechanical assessment

On the 35th day of culture, we measured the wall thickness, outer diameter, and length of the 3D-printed tubular structures (all groups, N = 3–5 per group) and segments of 4 cartilage rings of 9-week-old male F344/Jcl rat cervical tracheas (N=4; CLEA, Tokyo, Japan) using a machine vision system (Gellex International, Tokyo, Japan). To measure pulling force, all structures were tested according to uniaxial tension (DMT, Ann Arbor, USA). Briefly, small, stainless steel pins served as grips for each individual structure. The structures were pulled in tension-to-failure at a rate of 50 μm/sec. Maximum loading forces were calculated and UTS were calculated from the pulling force by dividing the failure load by the cross-sectional area of the structures.

5.7. Biochemical analysis

Cartilaginous tubes consisting of all spheroid groups (N = 3–5), fibrous tubes consisting of group F-IV spheroids (N = 3), trachea-like tubes (N = 3), and native rat tracheas (N = 3) were digested in papain (P4762-25MG; Sigma-Aldrich, St. Louis, MO, USA) solution (250 μg/ml in 20 mM sodium phosphate, pH 6.5, containing 2 mM dithiothreitol and 1 mM ethylenediaminetetraacetic acid (EDTA)) for 24 h at 65 °C. GAG content was measured using a Blyscan kit (Biocolor, Belfast, Northern Ireland), and the relative cell number was determined by quantification of total DNA using Quant-iT Assay kits (Invitrogen, Carlsbad, CA, USA) according to the manufacturer's protocol.

5.8. Histology and immunohistochemistry

The structures were fixed in 10% masked formalin, (Japan Tanner Corporation, Osaka, Japan) embedded in paraffin, overnight, and sectioned along axial planes at 4 μm. Additionally, the trachea-like tubes were sectioned along vertical planes. Mounted tissue sections were deparaffinized, rehydrated and stained with hematoxylin-eosin to visualize cellular organization. The deposition and distribution of collagenous fiber and the main ECM component were determined by Masson's trichrome staining. Fast Green and Picrosirius Red dual staining (0.1% Fast Green FCF and 0.2% Direct Red 80 in picric acid) was used to visualize the deposition and distribution of collagenous and non-collagenous matrix components by light microscopy (Aperio ImageScope; Leica Biosystems, Wetzlar, Germany). Polarized light images of samples stained with Picrosirius Red were acquired by inverted microscopy. A linear polarizer was positioned between the light source and the specimen, and the analyzer between the specimen and the camera. Prior to image acquisition, the analyzer was rotated to obtain the maximum light diminishment. Small collagen I and III fibers appeared green under polarized light, while larger collagen I fibers appeared yellow.[14]

Alcian blue staining and light microscopy were used to visualize the deposition and distribution of GAG. Immunohistochemistry was performed using the Leica Bond III autostainer (Leica Biosystems) according to the manufacturer's protocols using the following primary antibodies: collagen II (1:200, rabbit polyclonal, plcab; Abcam, Cambridge, UK), collagen IV (1:50, mouse monoclonal, M0785; Dako, Glostrup, Denmark), CD31 (1:500, rabbit monoclonal, bs-195 R; Bioss, Boston, MA, USA), pan-cytokeratin (1:150, mouse monoclonal, ab7753; Abcam). Primary antibodies were detected using a Bond Polymer Refine Detection Kit with 3,3′-diaminobenzidine as a chromogen (DS9800; Leica Biosystems Newcastle Ltd, UK). All immunohistochemistry images were acquired using a light microscope (Aperio ImageScope; Leica Biosystems).

5.9 Animal model

5.9.1. Implantation of trachea-like tubes in rats

Three 9-week-old rats were used for this experiment. Four rings of each cervical trachea were dissected through a median cervicotomy (**Figure 7a**) and replaced with trachea-like tubes (**Figure 7b**) supported by silicon stents (7 mm long and 1.7 mm outer diameter; Kenis, Osaka, Japan). The rats were anesthetized with isoflurane (4%), and ketamine hydrochloride (85 mg/kg; Sankyo, Tokyo, Japan) maintained with isoflurane (2%). Proximal and distal end-to-end anastomoses were performed with 7-0 polypropylene interrupted sutures. The stent was secured with additional sutures, and the cervical incision was closed. Because the transplanted cells were human, the rats were bred under immunosuppression management with tacrolimus (0.5 mg/kg Prograf; Astellas Pharma Inc., Tokyo, Japan) and intratracheal secretion management with atropine sulfate (0.05 mg/kg; Wako Pure Chemical Industries, Ltd., Osaka, Japan) hypodermically once a day. At the end of this experiment, the wound was re-opened, both ends of the trachea-like tube were clamped, and the tube was removed. The animals were euthanized by inhalation of isoflurane overdose.

5.9.2. Animal care

This study was carried out in strict accordance with the recommendations in the Guide for the Care and Use of Laboratory Animals of the National Institutes of Health. The protocol was approved by the Institutional Animal Care and Use Committee of Nagasaki University (Approval number 1607261327). All efforts were made to minimize suffering.

5.10. Statistical analysis

Data are reported as means ± standard deviation (SD). One-way analysis of variance (ANOVA) was used to analyze the thickness, length, tensile strength, and GAG content in structures and native tracheas with JMP Pro 11.2 software (JMP, Tokyo, Japan). $P < 0.05$ was considered significant.

Supporting Information

Supporting Information is available from the Wiley Online Library or from the author.

Acknowledgments
This work was supported by a Japan Society for the Promotion of Science (JSPS) KAKENHI Grant-in-Aid for Scientific Research (C) JP26462147 and Scientific Research (B) JP18H02895 and by Public Trust Surgery Research Fund. Editorial support was provided by Editage, Cactus Communications.

Conflict of interest
Koichi Nakayama is a co-founder and a shareholder of Cyfuse. Cyfuse is the manufacturer of Regenova.

Received: ((will be filled in by the editorial staff))
Revised: ((will be filled in by the editorial staff))
Published online: ((will be filled in by the editorial staff))

References

[1] E. J. ten Hallers, G. Rakhorst, H. A. Marres, J. A. Jansen, T. G. van Kooten, H. K. Schutte, J. P. van Loon, E. B. van der Houwen, G. J. Verkerke, *Biomaterials*. **2004**, *25*, 1533.

[2] Gómez-Caro, A. Morcillo, R. Wins, L. Molins, G. Galan, V. Tarrazona, *Multimed. Man. Cardiothorac. Surg*. **2011**, *2011*, 1111.

[3] H. J. Welkoborsky, M. L. Hinni, H. Moebius, L. Bauer, H. Ostertag, *Ann. Otol. Rhinol. Laryngol*, **2014**, *123*, 25.

[4] H. C. Grillo, *Ann. Thorac. Surg*. **2002**, *73*, 1995.

[5] D. Wright, B. B. Graham, H. C. Grillo, J. C. Wain, D. J. Mathisen, *Ann. Thorac. Surg*. **2002**, *74*, 308.

[6] N. Okumura, T. Nakamura, T. Natsume, K. Tomihata, Y. Ikada, Y. Shimizu, *J. Thorac. Cardiovasc. Surg*. **1994**, *108*, 337.

[7] K. Omori, T. Nakamura, S. Kanemaru, R. Asato, M. Yamashita, S. Tanaka, A. Magrufov, J. Ito, Y. Shimizu, *Ann. Otol. Rhinol. Laryngol*. **2005**, *114*, 429.

[8] Fabre, F. Kolb, E. Fadel, O. Mercier, S. Mussot, T. Le Chevalier, P. Dartevelle, *Ann. Thorac. Surg*. **2013**, *96*, 1146.

[9] P. Macchiarini, P. Jungebluth, T. Go, M. A. Asnaghi, L. E. Rees, T. A. Cogan, A. Dodson, J. Martorell, S. Bellini, P. P. Parnigotto, S. C. Dickinson, A. P. Hollander, S. Mantero, M. T. Conconi, M. A. Birchall, *Lancet*. **2008**, *372*, 2023.

[10] C. A. Vacanti, K. T. Paige, W. S. Kim, J. Sakata, J. Upton, J. P. Vacanti, *J. Pediatr. Surg*. **1994**, *29*, 201.

[11] R. Satake, M. Komura, H. Komura, T. Kodaka, K. Terawaki, K. Ikebukuro, H. Komuro, H. Yonekawa, K. Hoshi, T. Takato, Y. Nakayama, *J. Pediatr. Surg*. **2016**, *51*, 244.

[12] H. Naito, T. Tojo, M. Kimura, Y. Dohi, W. H. Zimmermann, T. Eschenhagen, S. Taniguchi, *Interact. Cardiovasc. Thorac. Surg*. **2011**, *12*, 156.

[13] H. C. Grillo, *Surgery of the trachea and bronchi*, BC Cecker Inc, Hamilton, ON, Canada **2004**.

[14] L. Zhang, J Hu, KA Athanasiou, *Crit. Rev. Biomed. Eng.* **2009**, *37*, 1.

[15] K. Nakayama, in *Biofabrication: Micro-and Nano-fabrication, Printing, Patterning and Assemblies*, (Eds. Forgacs G, Wei S), William Andrew, Oxford, UK **2013**, 1–21.

[16] M. Itoh, K. Nakayama, R. Noguchi, K. Kamohara, K. Furukawa, K. Uchihashi, S. Toda, J. Oyama, K. Node, S. Morita, *PLoS One*. **2015**, *10*, e0136681.

[17] F. Berthod, L. Germain, N. Tremblay, F. A. Auger, *J. Cell Physiol.* **2006**, *207*, 491.

[18] P. Au, J. Tam, D. Fukumura, R. K. Jain, *Blood*. **2008**, *111*, 4551.

[19] S. Wang, C. Zhou, H. Zheng, Z. Zhang, Y. Mei, J. A. Martin, *Osteoarth. Cartil*. **2017**, *25*, 742.

[20] D. Taniguchi, K. Matsumoto, T. Tsuchiya, R. Machino, Y. Takeoka, A. Elgalad, K. Gunge, K. Takagi, Y. Taura, G. Hatachi, N. Matsuo, N. Yamasaki, K. Nakayama, T. Nagayasu, *Interact. Cardiovasc. Thorac. Surg*. **2018**, *26*, 745.

[21] A. D. Dikina, H. A. Strobel, B. P. Lai, M. W. Rolle, E. Alsberg, *Biomaterials*. **2015**, *52*, 452.

[22] P. Jungebluth, J. C. Haag, S. Sjöqvist, Y. Gustafsson, A. Beltrán Rodríguez, C. Del Gaudio, A. Bianco, I. Dehnisch, P. Uhlén, S. Baiguera, G. Lemon, M. L. Lim, P. Macchiarini, *Nat. Protoc*. **2014**, *9*, 2164.

[23] J. M. Kelm, V. Lorber, J. G. Snedeker, D. Schmidt, A. Broggini-Tenzer, M. Weisstanner, B. Odermatt, A. Mol, G. Zünd, S. P. Hoerstrup. *J. Biotechnol*, **2010**, *148*, 46.

[24] N. L'Heureux, N. Dusserre, G. Konig, B. Victor, P. Keire, T. N. Wight, N. A. Chronos, A. E. Kyles, C. R. Gregory, G. Hoyt, R. C. Robbins, T. N. McAllister, *Nat. Med.* **2016**, *12*, 361.

[25] T. A Gwyther, J. Z. Hu, A. G. Christakis, J. K Skorinko, S. M. Shaw, K. L. Billiar, M. W. Roll, *Cells Tissues Organs.* **2011**, *194*, 13.

[26] C. Norotte, F. S. Marga, L. E. Niklason, G. Forgacs, *Biomaterials.* **2009,** *30*, 5910.

[27] H. Yurie, R. Ikeguchi, T. Aoyama, Y. Kaizawa, J. Tajino, A. Ito, S. Ohta, H. Oda, H. Takeuchi, S. Akieda, M. Tsuji, K. Nakayama, S. Matsuda, *PLoS One*. **2017**, *13*, 12.

[28] T. Deuse, S. Schrepfer, F. Koch-Nolte, M. Haddad, E. Schwedhelm, R. Böger, H. Schäfer, C. Detter, H. Reichenspurner, *J. Heart Lung Transplant*. **2005**, *24*, 1844.

[29] H. Lu, T. Hoshiba, N. Kawazoe, I. Koda, M. Song, G. Chen, *Biomaterials*. **2011**, *32*, 9658.

[30] F. Dell'Accio, C. De Bari, F. P. Luyten, *Arthritis Rheum*. **2001**, *44*, 1608.

[31] A. Wenger, N. Kowalewski, A. Stahl, A. T. Mehlhorn, H. Schmal, G. B. Stark, G. Inkenzeller, *Cells Tissues Organs*. **2005**, *181*, 80.

[32] A. Dickhut, K. Pelttari, P. Janicki, W. Wagner, V. Eckstein, M. Egermann, W. Richter, *J. Cell Physiol*. **2009**, *219*, 219.

[33] L. Bian, D. Y. Zhai, R. L. Mauck, J. A. Burdick, *Tissue Eng. Part A*. **2011**, *17*, 1137.

[34] V. V. Meretoja, R. L. Dahlin, F. K. Kasper, A. G. Mikos, *Biomaterials*. **2012**, *33*, 6362.

[35] C. Acharya, A. Adesida, P. Zajac, M. Mumme, J. Riesle, I. Martin, A. Barbero, *J. Cell Physiol*. **2012**, *227*, 88.

[36] R. L. Dahlin, L. A. Kinard, J. Lam, C. J. Needham, S. Lu, F. K. Kasper, A. G. Mikos, *Biomaterials*. **2014,** *35*, 7460.

[37] L. Wu, J. C. Leijten, N. Georgi, J. N. Post, C. A. van Blitterswijk, M. Karperien, *Tissue Eng. Part A*. **2011**, *17*, 1425.

[38] A. Seguin, S. Baccari, M. Holder-Espinasse, P. Bruneval, A. Carpentier, D. A. Taylor, E. Martinod, *J. Thorac. Cardiovasc. Surg.* **2013**, *145*, 1297.

[39] P. Whittaker, *Microsc. Anal.* 1995, **44**, 15.

[40] J. M. Kelm, C. D. Sanchez-Bustamante, E. Ehler, S. P. Hoerstrup, V. Djonov, L. Ittner, M. Fussenegger, *J. Biotechnol*. **2005**, *118*, 213.

[41] F, A. Saleh, M. Whyte, P. G. Genever, *Eur. Cell Mater*. **2011**, *22*, 242.

[42] B. L. Proffen, C. M. Haslauer, C. E. Harris, M. M. Murray, *Connect. Tissue Res*. **2013**, *54*, 14.

[43] J. H. Choi, S. M. Lim, Y. I. Yoo, J. Jung, J. W. Park, G. J. Kim, *J. Cell. Biochem*. **2016**, *117*, 1145.

[44] E. Pöschl, U. Schlötzer-Schrehardt, B. Brachvogel, K. Saito, Y. Ninomiya, U. Mayer, *Development*. **2004**, *131*, 1619.

Figure Captions

Figure 1. Macroscopic analysis of cartilaginous tubes.

(a–g) Images of cartilaginous tubes from the indicated groups: C-I (a), C-II (b), C-IIIa (c), C-IIIb (d), C-IIIc (e), C-IV (f), C-V (g). Each hash mark on the ruler represents 0.5 mm. (h, i) Structure thickness (h) and length (i) of the cartilaginous tubes. (j, k) Mechanical analysis of the cartilaginous tubes expressed by the maximum load at failure (j) and ultimate tensile stress (UTS) during uniaxial testing (k). (l-n) Biochemical analysis of the cartilaginous tubes. GAG content (l), DNA content (m), and GAG normalized to DNA in harvested samples (n). Data represent means ± SD. * $P < 0.05$, ** $P < 0.01$

Figure 2. Histological and immunohistological analysis of cartilaginous tubes.

Cross-sections of cartilaginous tubes stained with Alcian blue (a, e, i, m, q, u, y). Immunohistological staining with anti-collagen II (b, f, j, n, r, v, z), anti-collagen IV (c, g, k, o, s, w, aa), or anti-CD31 antibodies (d, h, l, p, t, x, and bb). Group C-I (a–d), group C-II (e–h), group C-IIIa (i–l), group C-IIIb (m–p), group C-IIIc (q–t), group C-IV (u–x), and group C-V (y–bb). Scale bars = 300 μm.

Figure 3. Macroscopic analysis of fibrous tubes.

(a–d) Images of fibrous tubes from the indicated groups: F-I (a), F-II (b), F-III (c), F-IV (d). Each hash mark on the ruler represents 0.5 mm. (e, f) Structure thickness (e) and length (f) of fibrous tubes. (g, h) Mechanical analysis of cartilaginous tubes expressed by the maximum load at failure (g) and ultimate tensile stress (UTS) during uniaxial testing (h). Data represent means ± SD. * $P < 0.05$.

Figure 4. Histological and immunohistological analysis of fibrous tubes.

Cross-sections of fibrous tubes were stained with Masson's trichrome (a, f, k, p), Fast Green/Picrosirius Red (b, g, l, q), or Picrosirius Red and observed using polarized light microscopy (c, h, m, r). Immunohistological staining with anti-collagen IV (d, i, n, and s), or anti-CD31 antibodies (e, j, o, and t). Group F-I (a–e), group F-II (f–j), group F-III (k–o), and group F-IV (p–t). Scale bars = 300 μm.

Figure 5. Macroscopic analysis of trachea-like tubes.

(a–d) Images of trachea-like tubes. Day 0 (a), day 7 with "Kenzan" (b), day 7 without "Kenzan" (c), and day 35 (d). Each hash mark on the ruler represents 0.5 mm. (e, f) Structure thickness (e) and length (f) of fibrous tubes, cartilaginous tubes, trachea-like tubes, and native rat trachea. (g, h) Mechanical analysis of each sample expressed by the maximum load at failure (g) and ultimate tensile stress (UTS) during uniaxial testing (h). (i, j, and k) Biochemical analysis of cartilaginous tubes. GAG content (i), DNA content (j), and GAG normalized to DNA in harvested samples (k). Data represent means ± SD. * $P < 0.05$.

Figure 6. Histological and immunohistological analysis of trachea-like tubes.

Axial planes of trachea-like tubes were stained with hematoxylin-eosin (a), Masson's trichrome (b), and Alcian blue (c). Immunohistological staining with anti-collagen IV (d), anti-collagen IV (e), and anti-CD31 antibodies (f). (g) regions of interest magnified in (f). Small capillary formation is indicated with arrowheads. Scale bars = 300 μm.

Figure 7. Macroscopic and microscopic findings after tracheal transplantation.

Defects after trachea resection during the operation (a). Photograph of the surgical field after graft transplantation (b), day 7 (c), and day 35 (d) after transplantation (arrows: junction between the graft and the trachea). Vascularization, epithelialization, and collagen formation of the graft on day 7 (e–i) and day 35 (j–n). Hematoxylin-eosin staining of the graft (e and j;

the trachea-like tube is within the dotted line). Histological and immunohistological staining with anti-CD31 antibodies showing capillary-like tube formation in the graft (f and k). Immunohistological staining with anti-pan-cytokeratin antibodies showing that the epithelialization started on day 7 and extended to day 35 (g and l; arrowheads). The staining area of Alcian blue (h and m; arrowheads) and collagen II (i and n; arrowheads) became clearer in the trachea-like tubes over time. Scale bars = 200 μm (f and k), 400 μm (g and l), and 700 μm (h, i, m, and n).

Figure 8. The Regenova bio-3D printer system.

Schematic illustration showing the generation process for the tubes. Step 1: spheroid preparation with four cell types. Step 2: Bio-3D printing by the “Kenzan” method, three tube types were designed. Step 3: maturation with the proper medium flow. Step 4: transplantation to the rat.

Figure 1.

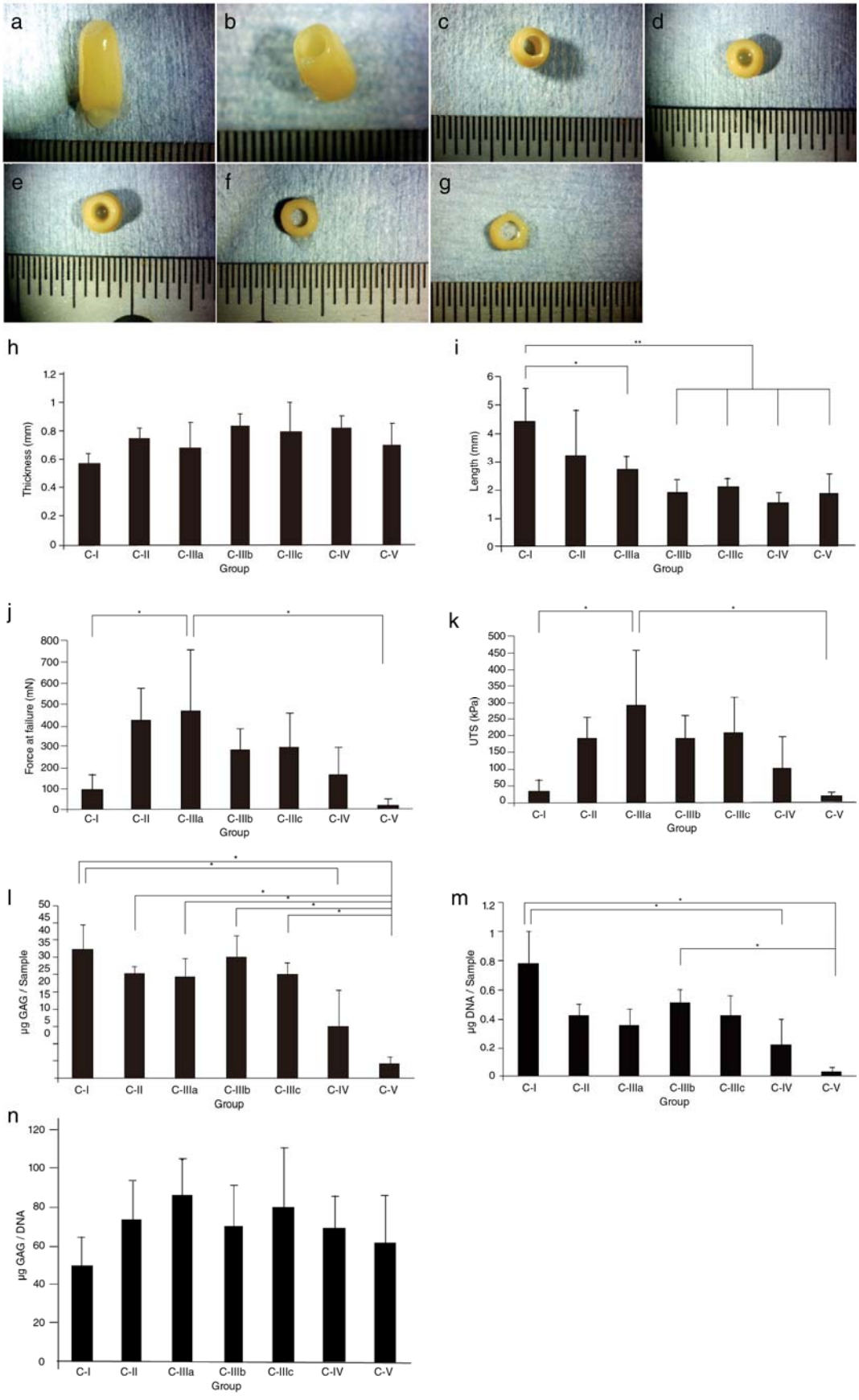
a
b
c
d
e
f
g
h
Thickness (mm)
C-I
C-II
C-IIIa
C-IIIb
C-IIIc
C-IV
C-V
Group
i
Length (mm)
j
Force at failure (mN)
k
UTS (kPa)
l
µg GAG / Sample
m
µg DNA / Sample
n
µg GAG / DNA

Figure 2.

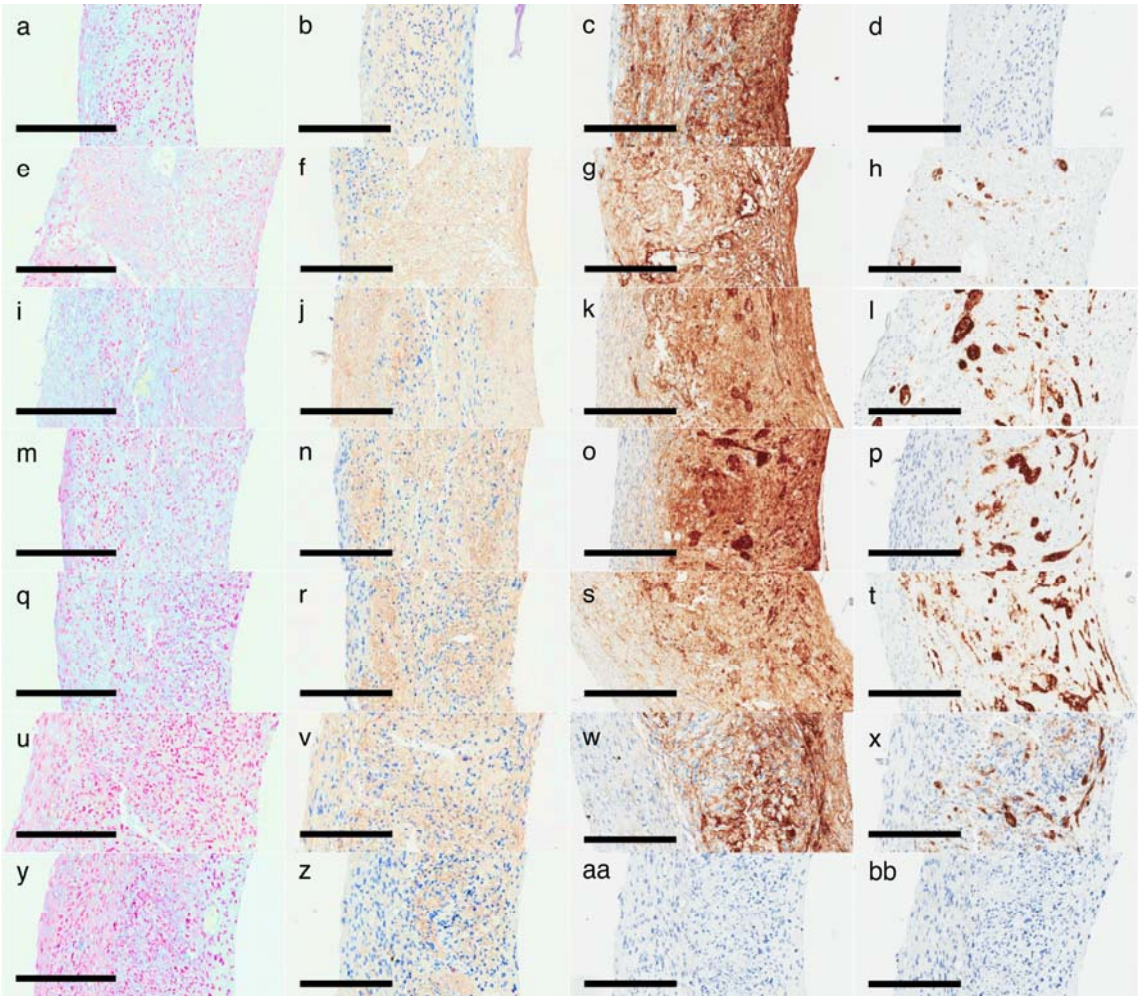

Figure 3.

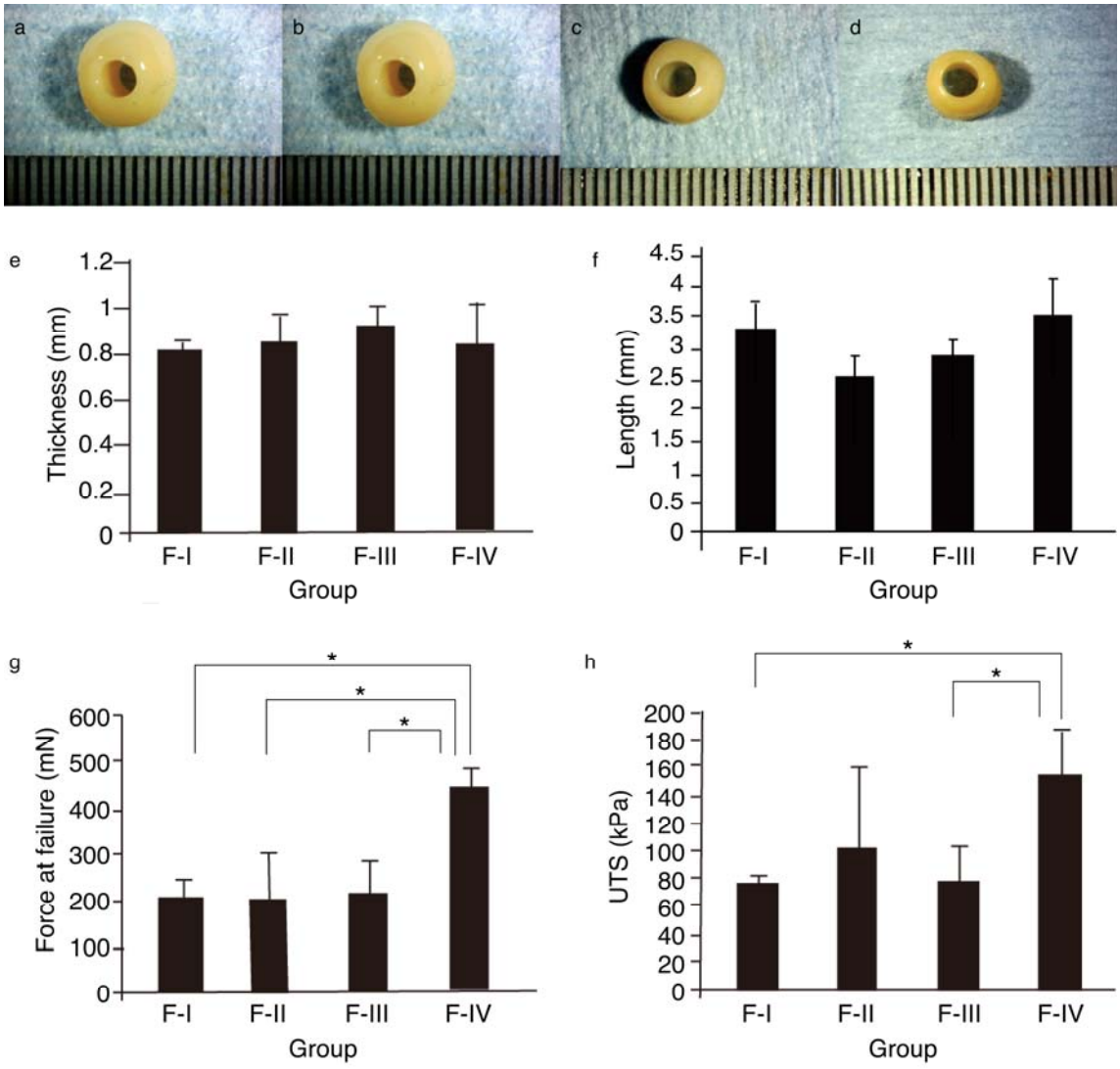
a
b
c
d
e
Thickness (mm)
1.2
1
0.8
0.6
0.4
0.2
0
F-I
F-II
F-III
F-IV
Group
f
Length (mm)
4.5
4
3.5
3
2.5
2
1.5
1
0.5
0
F-I
F-II
F-III
F-IV
Group
g
Force at failure (mN)
600
500
400
300
200
100
0
*
*
*
F-I
F-II
F-III
F-IV
Group
h
UTS (kPa)
200
180
160
140
120
100
80
60
40
20
0
*
*
F-I
F-II
F-III
F-IV
Group

Figure 4.

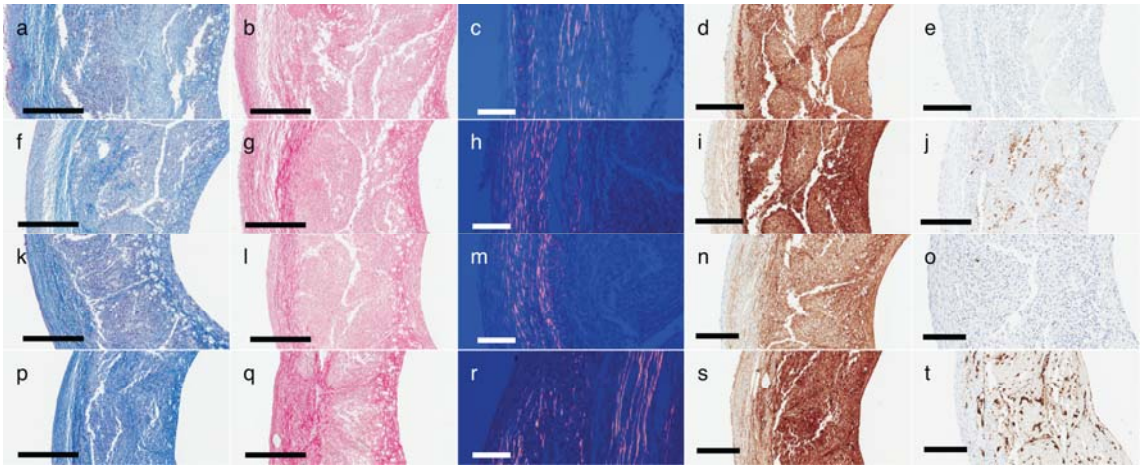

Figure 5.

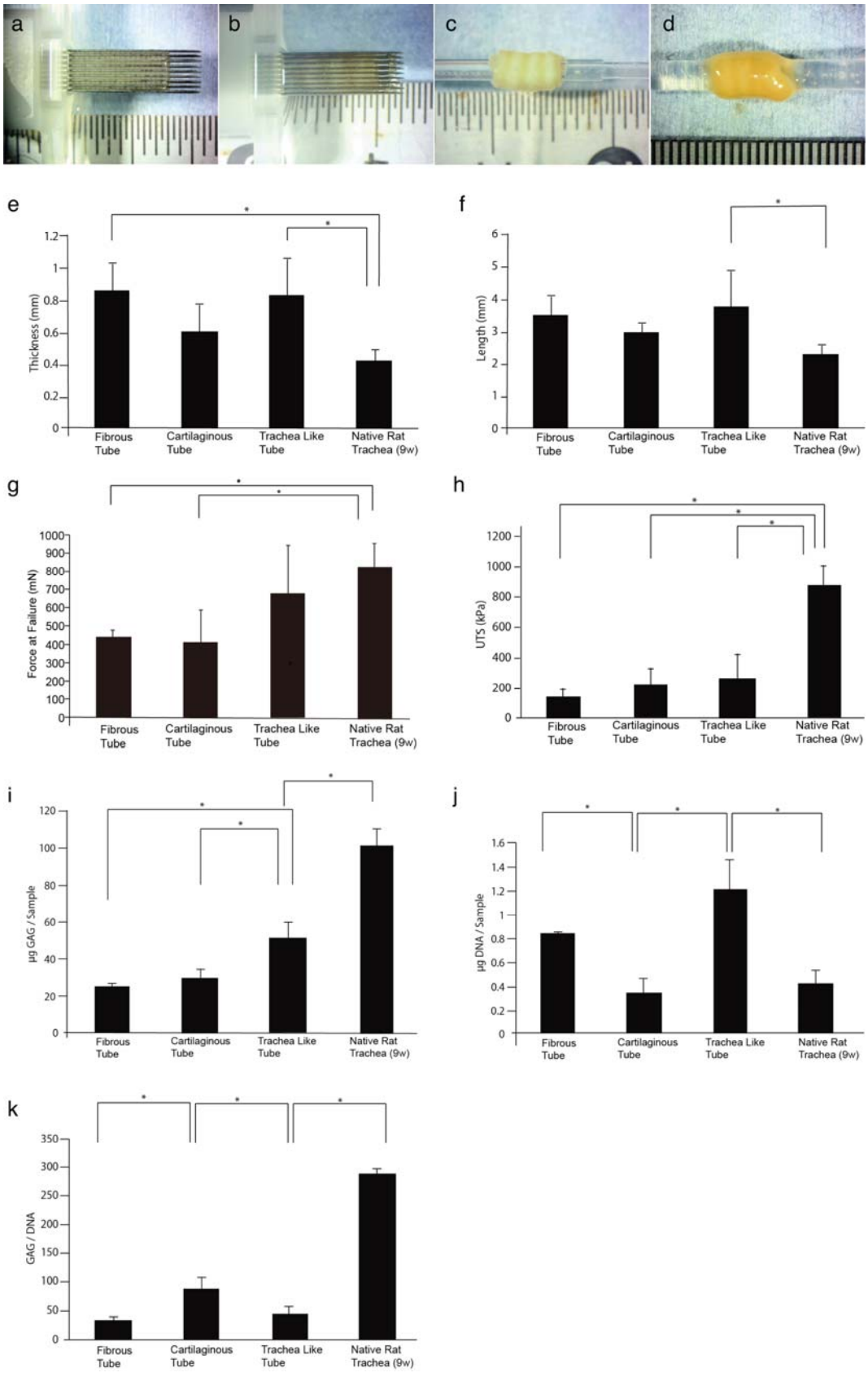
a
b
c
d
e
Thickness (mm)
1.2
1
0.8
0.6
0.4
0.2
0
Fibrous Tube
Cartilaginous Tube
Trachea Like Tube
Native Rat Trachea (9w)
f
Length (mm)
6
5
4
3
2
1
0
Fibrous Tube
Cartilaginous Tube
Trachea Like Tube
Native Rat Trachea (9w)
g
Force at Failure (mN)
1000
900
800
700
600
500
400
300
200
100
0
Fibrous Tube
Cartilaginous Tube
Trachea Like Tube
Native Rat Trachea (9w)
h
UTS (kPa)
1200
1000
800
600
400
200
0
Fibrous Tube
Cartilaginous Tube
Trachea Like Tube
Native Rat Trachea (9w)
i
µg GAG / Sample
120
100
80
60
40
20
0
Fibrous Tube
Cartilaginous Tube
Trachea Like Tube
Native Rat Trachea (9w)
j
µg DNA / Sample
1.6
1.4
1.2
1
0.8
0.6
0.4
0.2
0
Fibrous Tube
Cartilaginous Tube
Trachea Like Tube
Native Rat Trachea (9w)
k
GAG / DNA
350
300
250
200
150
100
50
0
Fibrous Tube
Cartilaginous Tube
Trachea Like Tube
Native Rat Trachea (9w)

Figure 6.

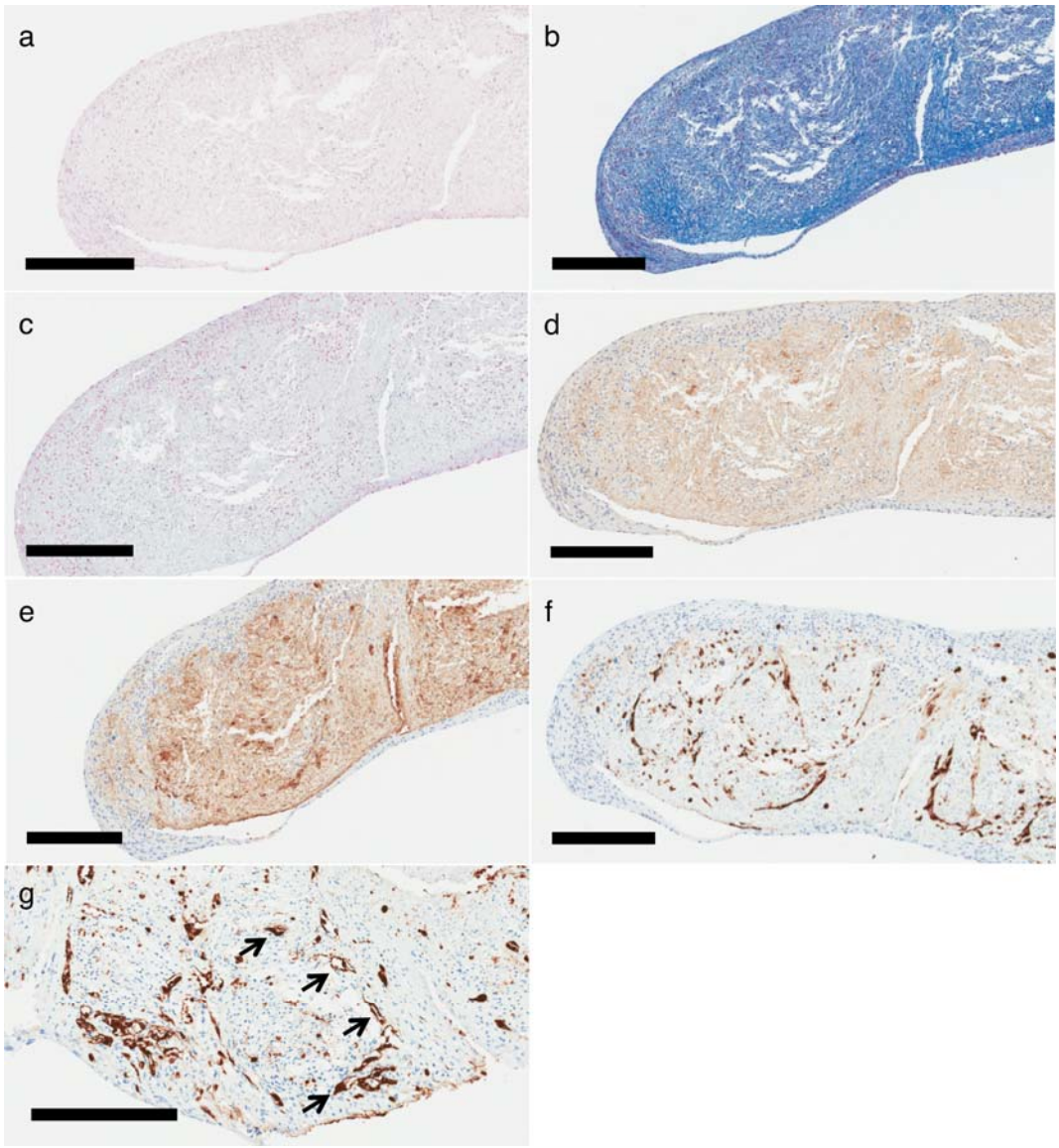

Figure 7.

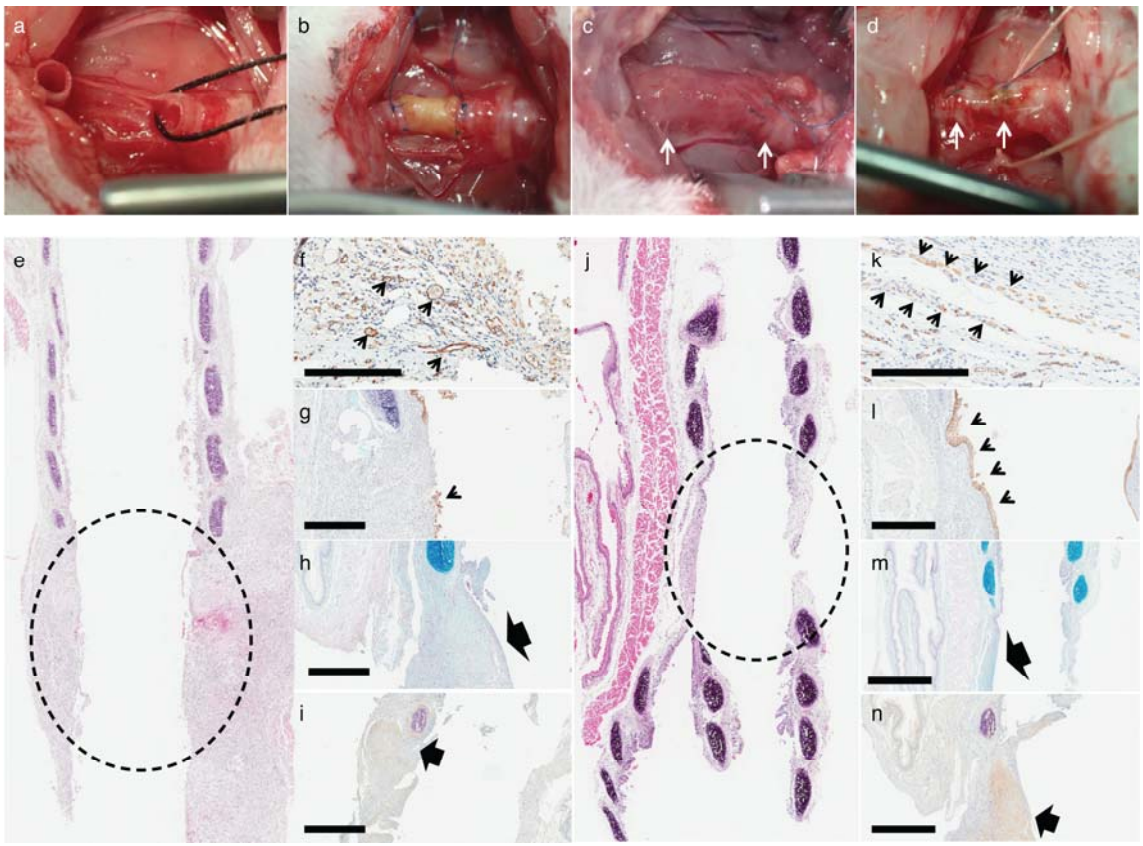

Figure 8.

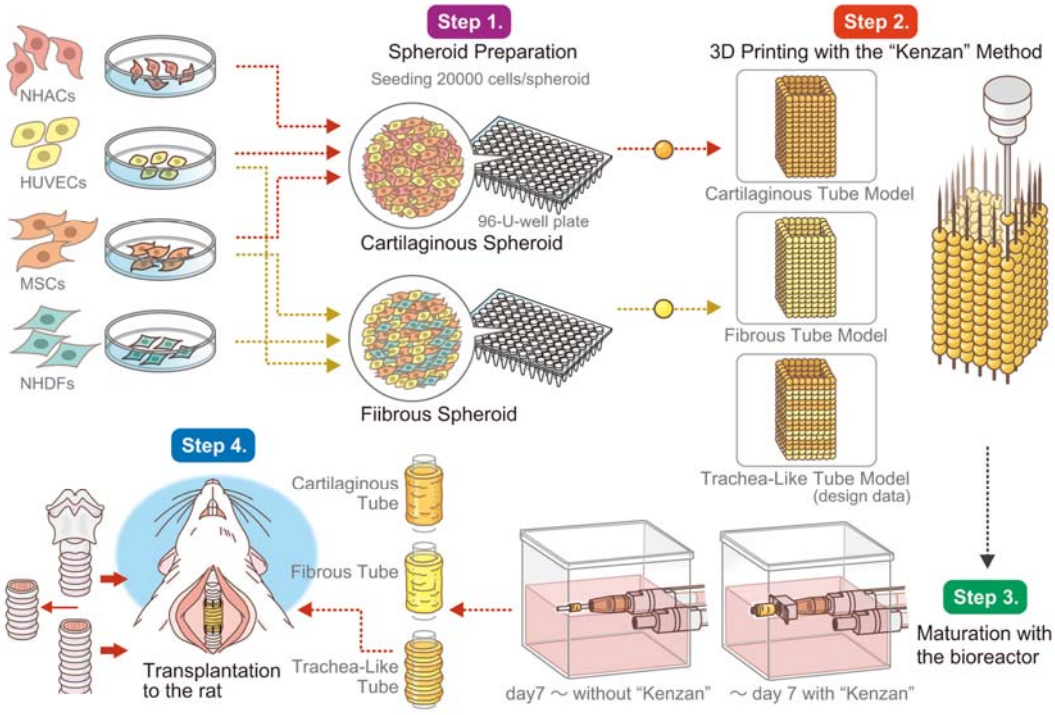
Step 1.
Spheroid Preparation
Seeding 20000 cells/spheroid
NHACs
HUVECs
MSCs
NHDFs
96-U-well plate
Cartilaginous Spheroid
Fiibrous Spheroid
Step 2.
3D Printing with the "Kenzan" Method
Cartilaginous Tube Model
Fibrous Tube Model
Trachea-Like Tube Model
(design data)
Step 3.
Maturation with
the bioreactor
day7 ~ without "Kenzan"
~ day 7 with "Kenzan"
Step 4.
Cartilaginous
Tube
Fibrous Tube
Trachea-Like
Tube
Transplantation
to the rat

Supporting Information

Replacement of Rat Tracheas by Layered, Trachea-like, Scaffold-free Structures of Human Cells Using Bio-3D Printing System

*Ryusuke Machino, Keitaro Matsumoto, Daisuke Taniguchi, Tomoshi Tsuchiya, Yosuke Takeoka, Yasuaki Taura, Masaaki Moriyama, Tomoyuki Tetsuo, Shosaburo Oyama, Katsunori Takagi, Takuro Miyazaki, Go Hatachi, Ryoichiro Doi, Kosuke Shimoyama, Naoto Matsuo, Naoya Yamasaki, Koichi Nakayama, Takeshi Nagayasu**

Table S1. Combinatorial details of the cell types and media for the cartilaginous tubes and fibrous tubes.

	Cells				Medium		
Spheroid type	NHACs (%)	NHDFs (%)	HUVECs (%)	MSCs (%)	CGM (%)	FGM (%)	EGM (%)
Group C-I	100				50		50
Group C-II	80		20		50		50
Group C-IIIa	70		20	10	50		50
Group C-IIIb	40		20	40	50		50
Group C-IIIc	10		20	70	50		50
Group C-IV			20	80	50		50
Group C-V				100	50		50
Group F-I		100				50	50
Group F-II		80	20			50	50
Group F-III		90		10		50	50

Group F-IV	70	20	10	50	50